HHS Public Access

Author manuscript

Int J Cancer. Author manuscript; available in PMC 2016 May 25.

Published in final edited form as:

Int J Cancer. 2015 May 15; 136(10): 2341–2351. doi:10.1002/ijc.29301.

Chromosome instability in diffuse large B cell lymphomas is suppressed by activation of the noncanonical NF-κB pathway

Sampath Ramachandiran[1], **Arsene Adon**[2], **Xiangxue Guo**[1], **Yi Wang**[2], **Huichen Wang**[2], **Zhengjia Chen**[3], **Jeanne Kowalski**[3], **Ustun R. Sunay**[1], **Andrew N. Young**[4], **Theresa Brown**[5], **Jessica C. Mar**[6], **Yuhong Du**[7], **Haian Fu**[7], **Karen P. Mann**[4], **Yasodha Natkunam**[8], **Lawrence H. Boise**[1,9], **Harold I. Saavedra**[2], **Izidore S. Lossos**[10], and **Leon Bernal-Mizrachi**[1]

[1] Department of Hematology and Medical Oncology, Winship Cancer Institute of Emory University, Atlanta, GA

[2] Department of Radiation Oncology, Winship Cancer Institute of Emory University, Atlanta, GA

[3] Department of Biostatistics and Bioinformatics, Winship Cancer Institute of Emory University, Atlanta, GA

[4]Department of Pathology and Laboratory Medicine, Winship Cancer Institute of Emory University, Atlanta, GA

[5] Empire Genomics LLC, Buffalo, NY

[6] Department of Systems and Computational Biology, Albert Einstein College of Medicine of Yeshiva University, Bronx, NY

[7] Department of Pharmacology, Winship Cancer Institute of Emory University, Atlanta, GA

[8] Department of Pathology, Stanford University School of Medicine, Stanford, CA

[9] Department of Cell Biology, Winship Cancer Institute, Emory University, Atlanta, GA

[10] Department of Medicine, Division of Hematology-Oncology and Molecular and Cellular Pharmacology, Sylvester Comprehensive Cancer Center, University of Miami, Miami, FL

Abstract

Diffuse large B cell lymphoma (DLBCL) is the most common form of lymphoma in the United States. DLBCL comprises biologically distinct subtypes including germinal center-like (GCB) and activated-B-cell-like DLBCL (ABC). The most aggressive type, ABC-DLBCL, displays dysregulation of both canonical and noncanonical NF-κB pathway as well as genomic instability. Although, much is known about the tumorigenic roles of the canonical NF-kB pathway, the precise role of the noncanonical NF-kB pathway remains unknown. Here we show that activation of the noncanonical NF-κB pathway regulates chromosome stability, DNA damage response and centrosome duplication in DLBCL. Analysis of 92 DLBCL samples revealed that activation of the noncanonical NF-κB pathway is associated with low levels of DNA damage and centrosome

Correspondence to: Leon Bernal-Mizrachi, Department of Hematology and Medical Oncology, Winship Cancer Institute of Emory University, 1365 Clifton Road, C1152B, GA 30322, USA, Telephone: 404-778-1670, ; Email: lbernal@emory.edu

Additional Supporting Information may be found in the online version of this article.

amplification. Inhibiting the noncanonical pathway in lymphoma cells uncovered baseline DNA damage and prevented doxorubicin-induced DNA damage repair. In addition, it triggered centrosome amplification and chromosome instability, indicated by anaphase bridges, multipolar spindles and chromosome missegregation. We determined that the noncanonical NF-κB pathway execute these functions through the regulation of GADD45α and REDD1 in a p53-independent manner, while it collaborates with p53 to regulate cyclin G2 expression. Furthermore, this pathway regulates *GADD45α*, *REDD1* and cyclin G2 through direct binding of NF-κB sites to their promoter region. Overall, these results indicate that the noncanonical NF-κB pathway plays a central role in maintaining genome integrity in DLBCL. Our data suggests that inhibition of the noncanonical NF-kB pathway should be considered as an important component in DLBCL therapeutic approach.

Keywords

diffuse large cell lymphoma; NF-κB; chromosome stability

Diffuse large B cell lymphoma (DLBCL) is the most common lymphoma subtype in the United States, accounting for approximately 25,000 cases per year.[1,2] Genomic studies have identified two DLBCL subtypes that resemble normal cells from distinct stages of B cell differentiation, namely germinal center-like (GCB) and activated B-cell-like (ABC) DLBCL.[3,4] ABC DLBCL is characterized by aggressive clinical course and inferior overall survival.[3,4] These unfavorable clinical characteristics are strongly associated with dysregulation of signals such as the nuclear factor κB (NF-κB) pathway.[5–7] Both canonical and noncanonical NF-κB pathways are involved in DLBCL, either concomitantly or independent of one another. Although, advances have been made in understanding the role of the canonical NF-κB pathway in DLBCL, the precise role of its noncanonical counterpart remains to be established.

Mutations in NF-κB regulatory proteins are found in a significant number of ABC-DLBCL, indicating a substantial role for this signal in lymphomagenesis.[7–9] Signals generated from NF-κB activating mutations in *A20, CARD11, RANK* and other genes results in phosphorylation of upstream activators, IKKγ and NIK.[10] These subunits subsequently triggers the canonical and/or noncanonical NF-κB pathways by promoting processing of precursor proteins p105/NF-κB1 and p100/NF-κB2 to their corresponding mature forms, p50 and p52.[11] Both mature proteins heterodimerize with other NF-κB members (p65/Rel-A, c-Rel or Rel-B) and translocate to the nucleus where they regulate the expression of genes that influence B cell survival, proliferation, differentiation and immunoglobulin gene (Ig) editing.[12–14]

Controlled genetic instability is inherent to the physiologic processes responsible for producing Ig diversity in B cells. Two members of the noncanonical NF-κB pathway, Rel B and NF-κB2, directly influence Ig editing by altering class switch recombination.[14] For example, Rel-B is directly implicated in interleukin 4 (IL4)-mediated immunoglobulin IgG1 isotype production. In addition, NF-κB2 inactivating mutations lead to deficiencies in late B

cell differentiation and reduced immunoglobulin levels in common variable immunodeficiency patients and in transgenic mouse models.[15,16]

Unlike its normal counterpart, DLBCL undergo inappropriate editing of the Ig and targets non-Ig genes.[5] The resulting genomic instability increases cells susceptibility to acquire oncogenic mutations and chromosomal translocations in multiple genes such as *MYC*, *BCL6*, *PIM1* and *BCL2*.[5,17,18] Given the role of noncanonical NF-κB pathway in class switch recombination (CSR), it is likely that this pathway regulates signals involved in controlling DLBCL genome integrity. Here, we demonstrate that activation of the noncanonical NF-kB pathway impacts chromosome stability in DLBCL by regulating genes involved in DNA repair, generation of reactive oxygen species and cell cycle control such as *GADD45α*, *REDD1* and cyclin G2.

Material and Methods

Cell lines

The Burkitt lymphoma cell line Daudi as well as the germinal center (BJAB) and activated (RCK8) DLBCL cell lines were grown in RPMI medium supplemented with 10% fetal bovine serum, 1% L-glutamine, 1 mM sodium pyruvate and 50 μg/mL penicillin-streptomycin. The activated B cell DLBCL cell line OCI-LY3 was cultured in Iscove's medium supplemented with 20% fresh human plasma (Innovative Research, MI), 1% L-glutamine, 1 mM sodium pyruvate and 50 μg/mL penicillin-streptomycin.

Apoptosis studies and DNA content measurement

For apoptosis studies, 10^6 cells were treated with 2 μg/mL doxorubicin (Sigma-Aldrich, MO) for 1 h. Ten hours later, 1×10^5 cells were stained with Annexin V-Alexa Fluor 488 (Molecular Probes, NY). Live cells were measured with a FACScan flow cytometer (Becton Dickinson, NJ), quantitating Annexin V (–) cells.

Immunoblotting and super shift assay

Immunoblotting was performed as previously described.[19] The following antibodies were used: p100 (sc-7386), p105 (sc-7178), Rel-B (sc-226), Rel-A (sc-372), p53 (2876) and GAPDH (sc-137179), all from Santa Cruz Biotechnology, TX. Histone H3 (9715) antibody was purchased from Cell Signaling Technology, MA. Nuclear and cytoplasmic fractions were obtained following the nuclear extraction protocol (Active Motif, CA).

DNA-binding activity of NF-κB in the OCI-LY3 cell line was assessed using a supershift assay. Double-stranded consensus oligonucleotide sequences representing the NF-κB response element (5′-AGTTGAGGGGACTTTCCCAGGC-3′ and 3′-TCAACTCCCCTGAAAGGGT CCG-5′) were purchased from Promega, WI. Primers were labeled with γ^{32}P-ATP using T4 kinase. After the labeling reaction, the mixtures were cleared with G-50 minicolumns. Ten micrograms of OCI-LY3 nuclear extract was incubated overnight with the radiolabeled probes and 2 μL Rel-A or Rel-B antibody and electrophoresed at 4°C (150 V) for 90 min on a 5% polyacrylamide gel containing 50 mM

Tris, pH 7.5, 0.38 M glycine and 2 mM EDTA. The gels were then processed for autoradiography.

Neutral Comet Assay

For DNA damage repair studies, 1×10^6 cells were treated with 2 μg/mL doxorubicin (Sigma-Aldrich, MO)) for 1 h. After washing in phosphate-buffered saline (PBS), cells were cultured in media and 20,000 cells were harvested at the indicated time points. Cells were suspended in 250 μl PBS at 4°C and mixed with 250 μl 1% low melting agarose (Lonza), then loaded onto a slide precoated with 1% agarose. The slides were immersed in lysis buffer (pH 9.5) containing 2.5 M NaCl, 100 mM EDTA, 10 mM Tris-HCl, 1% *N*-lauroylsarcosine, 0.5% Triton X-100 and 10% DMSO (freshly added), for overnight at 4°C. TBE (90 mM Tris, 90 mM boric acid, 2 mM Na_2EDTA [pH 8.5]) was used as rinse and electrophoresis buffer. After electrophoresis, slides were dried overnight at RT. The slides were then stained in a solution containing 50 mg/mL RNAse A and 40 mg/mL propidium iodide in PBS. Comets were analyzed using Kinetic Imaging analysis software (Andor Technology, UK). Olive tail moment (OTM) was used as an end point of DNA damage. OTM equals the tail length times the fraction of total DNA in the tail. Each bar represents the mean tail moment from at least 50 individual cells per time point of three independent experiments.

Plasmids

Sequences of p100-, p105- and p53-short hairpin RNA (shRNA) are published elsewhere.[19,20] The sense shRNA oligonucleotide probes were: Rel-B, 5′AGCCCGTCTATGACAAGAAAT3′; p105, 5′CCTTCCGCAAACTCAGCTTTA3′ and p100, 5′GCTGCTAAA TGCTGCTCAGAA3′ and 5′GGACATGACTGCCCAATT TAA3′. p53-shRNA was acquired from Addgene plasmid repository. Luciferase (Luc) shRNA plasmid was a kind gift of Dr. S.A. Stewart (Washington University in St. Louis, MO). Hairpins were expressed under U6 human promoter and were generated using pLKo carrying a puromycin cassette. Recombinant lentiviruses for infection of lymphoma cells were generated in 293T cells. Stable cell lines expressing shRNAs were obtained after selecting cells with 2 μg/mL puromycin.

In vitro immunofluorescence studies

Cells were placed onto slide using a cytospin techniques, and immunofluorescence was performed. Slides were fixed in cold 4% paraformaldehyde, permeabilized in 1% NP40/PBS solution for 10-15 min and blocked in 5% bovine serum albumin/PBS for 30 min. Chromosome breaks were detected using γ-H2AX antibody (1:250, ab22551, Abcam, MA). Centrosomes were detected using a γ-tubulin antibody at a 1:250 dilution (ab11317, Abcam, MA) and phospho-Aurora (2914, Cell signaling, MA) A. Anti Rel-A (sc-372) or Rel-B (sc-226) antibodies were purchased from Santa Cruz Biotechnology, TX. Primary antibodies were detected with the appropriate Alexa-488-conjugated secondary antibody (1:500, Molecular Probes, NY). Cells were also counterstained with 4, 6-diamidino-2-phenylindole (DAPI). For each experiment, 200 cells were counted per slide.

For analysis of chromosome migration, cells were harvested without metaphase arrest, stained with DAPI and analyzed in a blinded fashion. One hundred mitotic cells were included in each analysis. Anaphase bridges were defined as clear strings of chromatin connecting the two poles or stretching from one pole in the direction of the other pole and spanning more than two-thirds of the interpolar space. Spindles were scored as multipolar if they contained more than two foci of γ-tubulin staining. The frequency of anaphase bridges or multipolar spindles was calculated as the ratio between cells exhibiting such bridges and the total number of cells in anaphase.

Image acquisition, nuclear localization quantification and analysis in primary tissues

Images were acquired using a Zeiss LSM 510 META point scanning laser confocal microscope and captured by Zeiss Image LSM Browser (Integrated Cellular Imaging Core, Winship Cancer Institute of Emory University). Four images per sample were acquired in fields with a minimum of 200 cells. Quantification of the nuclear localization of Rel-A, Rel-B and γ-H2AX was performed using Metamorph software (Molecular Devices, CA)

Rel-A, Rel-B and γ-H2AX nuclear localization was quantified after performing a z-projection from the confocal images and transforming them into gray scale. The resulting images were processed using Metamorph software (Universal Imaging Corporation). Briefly, image processing started with sharpening and selecting the nuclear image (DAPI) based on size, avoiding large clumps and small debris. Each nucleus was used to create an object mask image, that later was dilated twice (×2 dilated). The twice-dilated image was subtracted from the original nuclear mask leaving a nuclear mask and a cytoplasmic mask. Subsequently, both masks were applied to the image containing the staining for the protein of interest. The threshold for the image was selected for each staining (Rel-A, Rel-B and γ-H2AX) to identify non-zero pixels. Measurements were then performed by obtaining the average intensity (AI, Supporting Information Figs. 1A and 1B).

Statistical analysis for correlation between Rel-A or Rel-B with γ-H2AX was performed using the following defined measurement of the overall average (among individual images) of the AI for each tissue:

$$AI = \frac{\sum_{i=1}^{4} Uj,i * Cj,i}{\sum_{i=1}^{4} cj,i}$$

where AI is the average of the average intensity per tissue, *j* is the sample, *i* is the image, *u* is the AI value and *c* is cell count. The correlation between Rel-A or Rel-B and γ-H2AX AI was estimated according to Spearman ranks correlation coefficient.

To assess the correlation between the number of centrosomes with Rel-A or Rel-B AI in primary tissues and in vitro experiments, we first quantified the number of centrosomes in >200 cells per tissue and calculated the percent of cells with ≥3 centrosomes per sample. Spearman's rank correlation coefficient was then evaluated between the percent of cells with ≥3 centrosomes and the AI for both NF-κB stains. To measure the number of γ-H2AX

positive cells in vitro, cells were stained with γ-H2AX as described above. The percent of cells with five or more γ-H2AX-positive nuclear foci were counted from 10 fields at each time point from three independent experiments. Statistically significant differences were calculated by analysis of variance.

Karyotype analysis

Metaphase chromosome preparation was performed by Empire Genomics, LLC, NY using standard cytogenetic techniques. Chromosome analysis was performed using Cytovision v7.3.2 (Leica Biosystems, IL) and up to 20 G-banded cells were karyotyped for each cell line. The results were reported according to International System for Human Cytogenetic Nomenclature 2013 guidelines.

Statistical analysis of microarray data

Triplicate samples of OCI-LY3 or Daudi shRNA-expressing cells were used for comparative gene expression analysis. RNA was extracted from 50×10^6 cells using an RNeasy Mini kit (Qiagen, CA). Microarray hybridization was prepared by Cogenics, using an Agilent 4X44 platform. Scanning and image analysis were performed using an Agilent 2100 Bioanalyzer and Agilent MR-2 DNA Microarray Scanner (Agilent Technologies). Raw data were processed using the statistical software R and BioConductor packages. First, raw data were log2-transformed and normalized using quantile normalization.[21] Second, we assessed for differential expression between cells expressing p100- or p105- and Luciferase-shRNA by implementing linear model and empirical Bayes statistics (Limma package[22,23]). *p* values were adjusted for multiple testing using the Benjamini-Hochberg method. Using a false discovery rate of 0.001, we selected a set of genes highly affected by the expression of p100- or p105-shRNA, generating a pathway-specific gene list.[24] Third, genes with inconsistent expression between OCI-LY3 and Daudi shRNA-expressing cells were filtered out. Subsequently, to account for the potential overlap between pathways, the remaining p100- or p105-regulated genes were compared and genes exclusively regulated by p100 were selected for confirmation by quantitative polymerase chain reaction (qPCR). A subsequent analysis performed by Cogenics company using GeneSpring GX software (Agilent Technologies, CA) identified an additional four genes exclusively regulated by p100. The gene lists obtained from both analyses were used for complete linkage hierarchical clustering analysis of the p100- and p105-shRNA microarray data using correlation as the distance metric (Made4 package[25]). The microarray data generated in our study have been deposited in the NIH Gene Expression Omnibus database under accession number GSE24020.

qPCR and mRNA analysis

Single strand cDNA was synthesized using 5 μg of total RNA, random hexamers and *Taq Man* reverse transcription reagents (Applied Biosystems, NY). Relative gene expression levels were measured using power SYBR green master mix (Bio-Rad, CA) and ABI PRISM 7000 sequence detection system. Primers were obtained from Integrated DNA Technologies, IA (Supporting Information Table 1A). Amplification efficiency of individual primers was determined before performing qPCR. The relative expression level of each gene was measured by QPCR as described by Pfaffl.[26] GAPDH was used as the reference gene.

Quantitative chromatin immunoprecipitation

Fifty million OCI-LY3 cells were harvested after 60 min of doxorubicin treatment, fixed with 1% formaldehyde and quenched with 0.125 M glycine. Chromatin was isolated by adding lysis buffer, followed by disruption with dounce homogenizer. Lysates were sonicated and DNA was sheared to an average length of 300–500 bp. Genomic DNA (Input) was prepared by treating aliquots of chromatin with RNase, proteinase K and heat for de-crosslinking, followed by ethanol precipitation.

Thirty micrograms of chromatin was precleared with protein A agarose beads (Invitrogen, NY). Genomic DNA regions were isolated using a p100 antibody (Abcam, ab7972, MA) or nonimmune IgG from the same species as the p100 antibody. The resulting signals were normalized for each primer efficiency (Supporting Information Table 1C).[26,27] Results are expressed as ratios of the real-time PCR signals obtained for IP with p100 antibody to those obtained from IgG. The relative occupancy of the immunoprecipitated factor at each locus was measured using the following equation: $2\text{^}(C_{\text{t mock}}$ [IgG] − $C_{\text{t specific}}$ [p100 antibody]), where $C_{\text{t mock}}$ and $C_{\text{t specific}}$ are mean threshold cycles of PCR done in triplicate on DNA samples from mock and specific immunoprecipitation. Results are presented as mean values with corresponding standard deviations.

Results

Rel-B nuclear localization inversely correlates with DNA damage and centrosome amplification in DLBCL tissues

To examine an association between the NF-κB pathways and genome stability, we examined the activation status of the canonical and noncanonical NF-κB pathways, levels of DNA damage and centrosome numbers in 92 primary DLBCL diagnostic specimens. To this end, we measured nuclear levels of Rel-A and Rel-B as indicators of canonical and noncanonical NF-κB activation, phosphorylation levels of the H2AX-carboxy-terminus (serine 139, γ-H2AX) as a measure of DNA damage and γ-tubulin as a centrosome marker to quantify the number of centrosomes (centrosomal amplification was defined as cells with ≥3 centrosomes). An inverse correlation was detected between Rel-B nuclear AI and either γ-H2AX AI or the proportion of cells with ≥3 centrosomes in the DLBCL tumor samples ($p < 0.0001$, Figures 1*a* and 1*b* right panels and Supporting Information Fig. 1A). In contrast, no significant correlation was detected between Rel-A and γ-H2AX AI, while a small but significant positive correlation was found between Rel-A AI and the proportion of cells with ≥3 centrosomes (Figs. 1*a* and 1*b* left panels). Furthermore, none of the four cases that concomitantly demonstrated high levels of Rel-A and Rel-B displayed high levels of γ-H2AX AI or an increase in the proportion of cells with ≥3 centrosomes (data not shown), suggesting the absence of a cooperative effect between these pathways. Finally, we evaluated the association between DLBCL subtypes (ABC *vs.* GCB cell-like) and DNA damage levels, centrosome numbers and Rel A and Rel B AI in 44 cases with previously established DLBCL subclassification (data not shown).[28] Our analysis was unable to detect any relationship between tumor subtype and these categories.

In view of the inverse correlation between activation of the noncanonical NF-κB pathway (Rel-B levels) and DNA damage and centrosome amplification in primary tumor samples, we investigated whether these results were reproducible in vitro. Three cell lines with documented NF-kB activation (ABC cell lines OCI-LY3 and RCK8 and Burkitt lymphoma cell line Daudi) and two cell lines without NF-kB activation (GCB DLBCL cell lines OCI-LY2 and SUDHL10)[19,29] were used to evaluate the effect of noncanonical NF-κB inhibition on DNA damage and centrosome numbers. First, we assessed the effect of silencing p100 expression (a member of the noncanonical NF-κB pathway) on DNA double strand breaks by measuring the number of cells positive for γ-H2AX and OTM in neutral comet assay. In NF-κB-activated cells, silencing of p100 not only reduced Rel-B binding to γ^{32}-P-labeled double stranded oligonucleotides (Supporting Information Fig. 2A),[19] demonstrating an inhibitory effect on the noncanonical NF-κB pathway but also increased the number of γ-H2AX (+) cells and OTM compared to cells expressing a control shRNA (Figs. 2*a*–2*c* and Supporting Information Fig. 2A4–C, $p < 0.005$). A similar phenotype of DNA damage was observed in cells without activation of NF-κB; however, this effect was not as pronounced. Next, the impact of p100 silencing on centrosome duplication was determined by counting centrosomes, using γ-tubulin as a centrosome marker. Cells expressing control shRNA displayed centrosome amplification (≥3 centrosomes) in fewer than 5% of cells (Fig. 2*d* and Supporting Information Figs. 3A and 3B). In contrast, p100 silencing resulted in an increase in the proportion of cells with centrosome amplification (OCI-LY3: 9–15%, RCK8: 23–39%, Daudi: 34–44%, SUDHL10: 7–9% and OCI-LY2:10–17%). More importantly, p100 silencing did not affect the colocalization of phospho-Aurora and γ-tubulin in cells undergoing mitosis, an important regulatory mechanism for the centrosome cycle (Supporting Information Fig. 3B.1–2).[30] The effect on DNA damage and centrosome duplication observed in p100-silenced cells was reproduced when Rel B, another member of the noncanonical NF-κB pathway, was silenced in OCI-LY3 cells (Supporting Information Fig. 3C). Overall, these results establish the relationship between the noncanonical NF-κB pathway, DNA damage and centrosome amplification in primary DLBCL tumors and cell lines.

Inhibition of the noncanonical NF-κB pathway reduce DNA damage repair

To elucidate whether the noncanonical NF-kB pathway is engaged during DNA damage, we measured the nuclear localization of Rel-B during DNA damage induced by doxorubicin, a key agent in DLBCL's treatment. Following 1 h treatment with doxorubicin, Rel-B nuclear localization increased in OCI-LY3, RCK8 and Daudi cells (Fig. 3*a*), while in SUDHL10 or OCI-LY2 cells Rel B nuclear localization remained unchanged (Supporting Information Fig. 3D). These results indicate that in NF-kB activated cells, the noncanonical pathway is engaged during the DNA damage response. Next, we determined whether activation of this NF-κB pathway influenced the levels of DNA damage by regulating DNA repair. To achieve this goal, we measured the ability of p100-silenced cells to recover from doxorubicin-induced DNA damage. In OCI-LY3, RCK8 and Daudi cells expressing control-shRNA, baseline low DNA damage levels rapidly increased, peaked after 4–6 h and then declined to baseline levels (Fig. 3*b*). In contrast, in p100-silenced cells, doxorubicin increased or maintained the initially high levels of DNA damage observed at baseline (Fig. 3*b* and Supporting Information Figs. 3A and 3B). These results were reproduced when shRNA

expressing Daudi and OCI-LY3 cells were treated with irradiation (3 Gy) (Supporting Information Fig. 4C). The differences in DNA damage levels observed between p100- and control-shRNA expressing cells likely reflect a difference in their DNA repair capacity, since apoptosis was not observed even after 10 h of doxorubicin treatment in all shRNA-expressing cells (Supporting Information Fig. 4D).

The response to DNA damage of cells without activation of NF-kB contrasted significantly to those with NF-kB activation. Specifically, p100-silencing in OCILY-2 and SUDHL10 cells led to earlier increases of doxorubicin-induced DNA damage as measured by phospho-γH2AX than controls (1–2 h *vs.* 4–6 h, respectively). However, this difference dissipated at 10 h when both control and p100 silenced cells reach peak DNA damage levels. In contrast, neutral comet assay showed little to no difference in tail moment among shRNA expressing cells. In both control and p100-silenced cells, tail moment peaked at 4 h and decreased at 10 h (Supporting Information Fig. 4E). Similar to previous reports describing that the contrast between these methods of DNA damage detection can result from the chromatin condensation observed during apoptosis,[31] we observed in SUDHL10 and OCI-LY2 higher rates of apoptosis compared to NF-kB activated cell lines (Supporting Information Fig. 4E).

Silencing of p100 is associated with cytokinesis failure

We hypothesized that the presence of DNA damage and centrosome amplification resulting from p100 silencing may predispose cells to cytokinesis failure and accumulation of genetic alterations in the form of mutations, aneuploidy and hyperdiploidy. We therefore evaluated the presence of chromosomal segregation defects in OCI-LY3, RCK8 and Daudi cells after silencing p100. Consistent with the presence of centrosome amplification, p100 silencing was more frequently associated with anaphase bridges and multipolar spindles (Figs. 4*a* and 4*b*). Furthermore, karyotype analysis and chromosome banding revealed that p100 silencing led to nondis-junction of chromatids. p100 silencing substantially increased the rate of chromosome misdivision in OCI-LY3, RCK8 and Daudi cells compared to controls (Figs. 4*c*–4*e* and Supporting Information Table 1C). In addition, p100-silenced OCI-LY3 and Daudi cells gained new translocations such as t(14;18) and t(8;14), respectively. This variety of structural and numerical chromosome abnormalities generated by silencing p100 validates the effect of the noncanonical NF-κB pathway on genome stability.

p100 regulates *GADD45a*, *CCNG2* and *REDD1* expression

Since the inactivation of the noncanonical NF-κB pathway increased DNA damage, centrosome amplification and aneuploidy, we examined potential mechanisms by which the noncanonical NF-κB pathway executes these functions. To this end we compared gene expression profiles of p100- or p105-silenced cells with their respective controls, to identify DNA repair and centrosome duplication genes regulated by the noncanonical NF-κB pathway. First, we documented the NF-κB inhibitory specificity of p100- and p105-shRNA by gel retardation assay and demonstrated that the binding of γ32P-labeled oligonucleotides by Rel-B was reduced primarily by p100 silencing, while Rel-A binding was primarily reduced by p105 silencing (Supporting Information Fig. 2A).[19] Next, we performed gene expression analysis and identified genes differently expressed when p100 or p105 were silenced in OCI-LY3 and Daudi cells (Fig. 5*a*). Among the genes regulated in both OCI-LY3

and Daudi cell lines, eight genes affected by p100-shRNA are associated with DNA repair and centrosome duplication. Changes in expression of five of these genes were validated by qPCR (see Supporting Information Table 1D).

In an effort to identify which of these genes participate in the NF-κB-mediated DNA damage response, we measured their mRNA levels in control or p100-silenced OCI-LY3 cells following treatment with doxorubicin. Of these five genes, only expression levels of growth arrest and DNA-damage-inducible 45 alpha (*GADD45α*), cyclin G2 (*CCNG2*) and DNA-damage-inducible transcript 4 (*REDD1*) were induced (≥2-fold) by doxorubicin in control cells. However, when p100 was silenced, doxorubicin's induction of *GADD45α*, *CCNG2* and *REDD1* mRNA expression was prevented (Fig. 5*b*).

p100 regulates *GADD45α* and *REDD1* in a p53-independent manner

Since all three p100-regulated genes identified can also be regulated by p53, it is possible that p100 induces these genes through p53. To differentiate whether these genes are directly regulated by p100/p52 or indirectly through p53, we measured the mRNA levels of these genes in p53 wild type cells (OCI-LY3) expressing p53-shRNA during doxorubicin treatment. *GADD45α* and *REDD1* expression increased following 60 min of treatment despite p53 silencing (Fig. 5*c* and Supporting Information Fig. 5A). On the other hand, *CCNG2* expression levels at 60 min were reduced compared to that seen in control cells, suggesting that both p100 and p53 regulate *CCNG2* expression (Fig. 5*c*). The effect of p53 silencing was validated by the lack of doxorubicin-induced expression of p21 (Supporting Information Fig. 5B). Furthermore, similar increases in the mRNA levels of *GADD45α*, *REDD1* and *CCNG2* were observed after doxorubicin treatment of a p53-mutant BJAB DLBCL cell line (Supporting Information Fig. 5C).[32] Taken together, these data suggest that p100 directly and independent of p53 regulates *GADD45α* and *REDD1* expression, while *CCNG2* appears to be regulated by both p100 and p53. This possibility was further evaluated by quantitative chromatin immunoprecipitation (qCHIP)[27] in OCI-LY3 cells following a 60-minute treatment with doxorubicin. Our data demonstrate that p100/p52 binds to the NF-κB *cis*-elements in the promoter regions of *REDD1*, *GADD45α* and *CCNG2* (Fig. 5*d*). Binding of NF-κB2 subunits to unrelated sequences in chromosome 4 (untranscribed region) and IP without p100/p52 antibody were indistinct from background levels. These results confirm that p100 directly regulates the expression of *GADD45α*, *REDD1* and *CCNG2*.

Based on p100's specific regulation of *GADD45α* and *REDD1*, we individually silenced *GADD45α* and *REDD1* to determine if either of these genes is the primary mediator of p100's DNA damage response. Accordingly, we measured the number of γ-H2AX (+) cells and centrosomes in *GADD45α*- or *REDD1*-silenced OCI-LY3 cells. Figures 6*a* and 6*b* show that silencing of either *GADD45α* or *REDD1* led to a higher number of γ-H2AX (+) cells. In addition, silencing of *GADD45α* but not *REDD1* was associated with an increased number of centrosomes (Figs. 6*a* and 6*b*).

Discussion

In our study, we provide evidence that activation of the noncanonical NF-κB pathway participates in maintaining DLBCL genome integrity by enhancing DNA repair and suppressing centrosome amplification. We have demonstrated that the noncanonical NF-κB pathway performs these functions by directly regulating the transcription of genes involved in cell cycle regulation and DNA repair, such as *GADD45a*, *REDD1* and *CCNG2*. This novel observation improves our understanding of DLBCL biology and has direct implication for therapeutic applications targeting DLBCL's dependency on noncanonical NF-κB pathway to control genomic instability (Fig. 6*c*).

We have provided three independent lines of evidence demonstrating the involvement of the noncanonical NF-κB pathway in suppressing DLBCL genomic instability. First, studies in primary tissues displayed an inverse correlation between activation of the noncanonical NF-κB pathway (assayed by Rel-B nuclear localization) and DNA damage and centrosome amplification. Second, NF-κB inhibition through p100- or Rel-B-silencing uncovered the presence of tonic DNA damage as well as promoted centrosome amplification in lymphoma cell lines. Third, NF-κB inhibition through p100 silencing led to increased rates of aneuploidy.

We propose a potential mechanism by which the noncanonical NF-κB pathway suppresses genomic instability. We found that the noncanonical NF-κB pathway regulated transcription of genes involved in maintaining genome integrity (*GADD45a*, *CCNG2 and REDD1*) through direct interaction with their promoter regions. The regulation of *GADD45a* and *REDD1* in a p53-independent manner was unexpected, since p100-dependent transcriptional regulation of *GADD45a* has been proposed to require p53 as a coactivator.[33,34] However, our findings of reduced *GADD45a* and *REDD1* expression in p100-silenced lymphoma cells during DNA damage, preserved expression of these genes in cells with silenced or mutated p53, and p100 promoter binding analyses allow us to place these genes directly downstream of the noncanonical NF-κB pathway (Fig. 6*c*).

The fact that we could not demonstrate that *GADD45a* and *REDD1* individually mediate the effect of NF-κB on DNA repair response is potentially due to their collaborative function in preserving genome integrity. *GADD45a* regulates G2/M checkpoints and the entry to mitosis by dissociating the Cdk1/cyclin B kinase complex.[35] Moreover, *GADD45a* participates in DNA repair by binding and activating the proliferating cell nuclear antigen, a key element in excision base repair.[36] In contrast, *CCNG2* is directly involved in coordinating G1-S progression by altering RB activation.[37,38] Thus, by controlling these two genes, the noncanonical NF-κB pathway may affect the duration of DNA synthesis and the centrosome duplication process. In addition, *REDD1* controls the generation of reactive oxygen species and therefore prevents further DNA damage.[39,40]

Our findings in DLBCL shed light on a dual function of the noncanonical NF-κB pathway in tumor prevention and maintenance. The inverse correlation between the activation status of the noncanonical NF-κB pathway (Rel-B nuclear localization) and genome instability observed in primary DLBCL tissues is consistent with the high risk of lymphoma in ataxia

telangectasia patients.[41,42] As a consequence, this patient population demonstrates increased levels of DNA damage, accumulation of ROS and consistent with our results, NF-κB activation.[43,44] These findings are consistent with the idea that a dysregulated noncanonical NF-κB pathway-mediated DNA damage response can facilitate the selection of genetic alterations with tumorigenic capacity in normal lymphocytes. In established DLBCL, on the other hand, the noncanonical NF-κB pathway's suppressive effect on DNA damage response and centrosome duplication could be essential for maintaining tumor genome integrity and growth. The increase in DNA breaks associated with an overactive adenosine deaminase activity and the high frequency of mutations in DNA damage repair enzymes predispose DLBCL cells to chromosomal instability and cell death.[45,46] Hence, maintaining genome integrity prevents DLBCL from surrendering to the apoptotic effect of endogenous or chemotherapy-induced DNA damage.[45] In addition, activation of this pathway promotes growth by recruiting other NF-κB protumorigenic effects on survival, growth and invasion.[19] These observations make plausible the idea that pharmacological inhibition or genetic suppression of several G2 checkpoint genes such as poly ADP ribose polymerase, ATM, ATR, checkpoint kinase (Chk) 1, Chk2 and polo-like kinases, could promote DNA-damage-induced cell death in DLBCL.[47–50]

In summary, our study provides evidence that the noncanonical NF-κB pathway plays a pivotal role in guarding the genome. This finding provides a rationale for the design of therapies targeting DLBCL dependency on the noncanonical NF-kB to enhance response to DNA damaging agents.

Supplementary Material

Refer to Web version on PubMed Central for supplementary material.

Acknowledgements

The authors thank Dr. Sagar Lonial and Dr. Jean L. Koff for their critical review and helpful comments. This work was supported by the National Institutes of Health [CA15121 to H.I.S., CA109335 and CA122105 to I.S.L. and CA127910 and CA129968 to L.H.B]; the National Cancer Institute [K01CA104079 to H.I.S.]; Georgia Cancer Coalition Distinguished Scholar Award to H.I.S, L.H.B; Lymphoma Research Foundation and the Dwoskin Family, Recio Family and Anthony Rizzo Family Foundations to I.S.L. and Byron Davis Research Fund and Crissey Hematology and Medical Oncology Research Fund to L. B-M.

Grant sponsor: National Institutes of Health; **Grant numbers:** CA15121, CA109335, CA122105, CA127910 and CA129968; **Grant sponsor:** National Cancer Institute; **Grant number:** K01CA104079; Grant sponsors: Georgia Cancer Coalition Distinguished Scholar Award, Lymphoma Research Foundation and the Dwoskin Family, Recio Family and Anthony Rizzo Family Foundations, Byron Davis Research Fund and Crissey Hematology and Medical Oncology Research Fund; **Grant sponsor:** Emory University Integrated Cellular Imaging Microscopy Core and the Biostatistics and Bioinformatics Shared resource of the Winship Cancer Institute comprehensive cancer center; **Grant number:** P30CA138292

References

1. Altekruse, SF.; Kosary, CL.; Krapcho, M., et al. SEER Cancer Statistics Review 1975–2007. National Cancer Institute; 2010. SEER web site
2. Jemal A, Siegel R, Ward E, et al. Cancer Statistics, 2009. CA Cancer J Clin. 2009; 59:225–49. [PubMed: 19474385]
3. Alizadeh AA, Eisen MB, Davis RE, et al. Distinct types of diffuse large B-cell lymphoma identified by gene expression profiling. Nature. 2000; 403:503–11. [PubMed: 10676951]

4. Rosenwald A, Wright G, Chan WC, et al. The use of molecular profiling to predict survival after chemotherapy for diffuse large-B-cell lymphoma. N Engl J Med. 2002; 346:1937–47. [PubMed: 12075054]
5. Lenz G, Nagel I, Siebert R, et al. Aberrant immunoglobulin class switch recombination and switch translocations in activated B cell-like diffuse large B cell lymphoma. J Exp Med. 2007; 204:633–43. [PubMed: 17353367]
6. Staudt LM. Oncogenic activation of NF-κB. Cold Spring Harbor Perspect Biol. 2010:2.
7. Compagno M, Lim WK, Grunn A, et al. Mutations of multiple genes cause deregulation of NF-κB in diffuse large B-cell lymphoma. Nature. 2009; 459:717–21. [PubMed: 19412164]
8. Ngo VN, Young RM, Schmitz R, et al. Oncogenically active MYD88 mutations in human lymphoma. Nature. 2011; 470:115–19. [PubMed: 21179087]
9. Lohr JG, Stojanov P, Lawrence MS, et al. Discovery and prioritization of somatic mutations in diffuse large B-cell lymphoma (DLBCL) by whole-exome sequencing. Proc Natl Acad Sci USA. 2012; 109:3879–84. [PubMed: 22343534]
10. Wu Z-H, Shi Y, Tibbetts RS, et al. Molecular linkage between the kinase ATM and NF-kappaB signaling in response to genotoxic stimuli. Science. 2006; 311:1141–46. [PubMed: 16497931]
11. Schröfelbauer B, Polley S, Behar M, et al. NEMO ensures signaling specificity of the pleiotropic IKK^2 by directing its kinase activity toward IjBa. Mol Cell. 2012; 47:111–21. [PubMed: 22633953]
12. Verkoczy L, Aït-Azzouzene D, Skog P, et al. Role for nuclear factor Kappa B/Rel transcription factors in the regulation of the recombinase activator genes. Immunity. 2005; 22:519–31. [PubMed: 15845455]
13. Derudder E, Cadera EJ, Vahl JC, et al. Development of immunoglobulin [lambda]-chain-positive B cells, but not editing of immunoglobulin [kappa]-chain, depends on NF-[kappa]B signals. Nat Immunol. 2009; 10:647–54. [PubMed: 19412180]
14. Bhattacharya D, Lee DU, Sha WC. Regulation of Ig class switch recombination by NF-kaapaB: retroviral expression of RelB in activated B cells inhibits switching to IgG1, but not to IgE. Int Immunol. 2002; 14:983–91. [PubMed: 12202396]
15. Chen K, Coonrod Emily M, Kumánovics A, et al. Germline mutations in NFKB2 implicate the non-canonical NF-κB pathway in the pathogenesis of common variable immunodeficiency. Am J Hum Genet. 2013; 93:812–24. [PubMed: 24140114]
16. Tucker E, O'Donnell K, Fuchsberger M, et al. A novel mutation in the Nfkb2 gene generates an NF-jB2 “Super Repressor”. J Immunol. 2007; 179:7514–22. [PubMed: 18025196]
17. Pasqualucci L, Neumeister P, Goossens T, et al. Hypermutation of multiple proto-oncogenes in B-cell diffuse large-cell lymphomas. Nature. 2001; 412:341–46. [PubMed: 11460166]
18. de Miranda NF, Peng R, Georgiou K, et al. DNA repair genes are selectively mutated in diffuse large B cell lymphomas. J Exp Med. 2013; 210:1729–42. [PubMed: 23960188]
19. Bernal-Mizrachi L, Lovly CM, Ratner L. The role of NF-{kappa}B-1 and NF-{kappa}B-2-mediated resistance to apoptosis in lymphomas. PNAS. 2006; 103:9220–25. [PubMed: 16751281]
20. Godar S, Ince TA, Bell GW, et al. Growth-inhibitory and tumor-suppressive functions of p53 depend on its repression of CD44 expression. Cell. 2008; 134:62–73. [PubMed: 18614011]
21. Bolstad BM, Irizarry RA, Ãstrand M, et al. A comparison of normalization methods for high density oligonucleotide array data based on variance and bias. Bioinformatics. 2003; 19:185–93. [PubMed: 12538238]
22. Smith G. Linear models and empirical bayes methods for assessing differential expression in microarray experiments. Stat Appl Genet Mol Biol. 2004:3. Article 3.
23. Gentleman R, Carey V, Bates D, et al. Bioconductor: open software development for computational biology and bioinformatics. Genome Biol. 2004; 5:R80. [PubMed: 15461798]
24. Benjamini Y, Hochberg Y. Controlling the false discovery rate: a practical and powerful approach to multiple testing. J R Stat Soc Series B. 1995; 57:289–300.
25. Culhane A, Thioulouse J, Perriere G, et al. MADE4: an R package for multivariate analysis of gene expression data. Bioinformatics. 2005; 21:2789–90. [PubMed: 15797915]

26. Pfaffl M. A new mathematical model for relative quantification in real-time RT-PCR. Nucleic Acids Res. 2001; 29:2003–7. [PubMed: 11353068]
27. Mukhopadhyay A, Deplancke B, Walhout AJM, et al. Chromatin immunoprecipitation (ChIP) coupled to detection by quantitative real-time PCR to study transcription factor binding to DNA in Caenorhabditis elegans. Nat Protoc. 2008; 3:698–709. [PubMed: 18388953]
28. Sarosiek KA, Malumbres R, Nechushtan H, et al. Novel IL-21 signaling pathway up-regulates c-Myc and induces apoptosis of diffuse large B-cell lymphomas. Blood. 2010; 115:570–80. [PubMed: 19965678]
29. Davis RE, Brown KD, Siebenlist U, et al. Constitutive nuclear factor {kappa}B activity is required for survival of activated B cell-like diffuse large B cell lymphoma cells. J Exp Med. 2001; 194:1861–74. [PubMed: 11748286]
30. Prajapati S, Yamamoto Y, Gaynor RB, et al. IKKalpha regulates the mitotic phase of the cell cycle by modulating Aurora A phosphorylation. Cell Cycle. 2006; 5:2371–80. [PubMed: 17102620]
31. Yu Y, Zhu W, Diao H, Zhou C, et al. A comparative study of using comet assay and γH2AX foci formation in the detection of N-methyl-N′-nitro-N-nitrosoguanidine-induced DNA damage. Toxicol in Vitro. 2006; 20:959–65. [PubMed: 16473493]
32. Bhatia K, Goldschmidts W, Gutierrez M, et al. Hemi- or homozygosity: a requirement for some but not other p53 mutant proteins to accumulate and exert a pathogenetic effect. FASEB J. 1993; 7:951–6. [PubMed: 8344493]
33. Schumm K, Rocha S, Caamano J, et al. Regulation of p53 tumour suppressor target gene expression by the p52 NF-kappaB subunit. Embo J. 2006; 25:4820–32. [PubMed: 16990795]
34. Barré B, Coqueret O, Perkins ND. Regulation of activity and function of the p52 NF-κB subunit following DNA damage. Cell Cycle. 2010; 9:4795–804. [PubMed: 21131783]
35. Liebermann D, Hoffman B. Gadd45 in stress signaling. J Mol Signal. 2008; 3:15. [PubMed: 18789159]
36. Hollander M, Fornace AJ. Genomic instability, centrosome amplification, cell cycle check points and Gadd45a. Oncogene. 2002; 21:6228–33. [PubMed: 12214253]
37. Bennin DA, Don ASA, Brake T, et al. Cyclin G2 associates with protein phosphatase 2A catalytic and regulatory B′ subunits in active complexes and induces nuclear aberrations and a G1/S phase cell cycle arrest. J Biol Chem. 2002; 277:27449–67. [PubMed: 11956189]
38. Arachchige Don A, Dallapiazza R, Bennin D, et al. Cyclin G2 is a centrosome-associated nucleocytoplasmic shuttling protein that influences microtubule stability and induces a p53-dependent cell cycle arrest. Exp Cell Res. 2006; 312:4181–204. [PubMed: 17123511]
39. Ellisen LW, Ramsayer KD, Johannessen CM, et al. REDD1, a developmentally regulated transcriptional target of p63 and p53, links p63 to regulation of reactive oxygen species. Mol Cell. 2002; 10:995–1005. [PubMed: 12453409]
40. Schneider A, Younis RH, Gutkind JS. Hypoxia-induced energy stress inhibits the mTOR pathway by activating an AMPK/REDD1 signaling axis in head and neck squamous cell carcinoma. Neoplasia. 2008; 10:1295–302. [PubMed: 18953439]
41. Taylor AM, Metcalfe JA, Thick J, et al. Leukemia and lymphoma in ataxia telangiectasia. Blood. 1996; 87:423–38. [PubMed: 8555463]
42. Jung M, Dritschilo A. NF-κB signaling pathway as a target for human tumor radiosensitization. Semin Radiat Oncol. 2001; 11:346–51. [PubMed: 11677659]
43. Jung M, Zhang Y, Lee S, et al. Correction of radiation sensitivity in Ataxia Telangiectasia cells by a truncated IκB-α. Science. 1995; 268:1619–21. [PubMed: 7777860]
44. Kamsler A, Daily D, Hochman A, et al. Increased oxidative stress in Ataxia Telangiectasia evidenced by alterations in redox state of brains from Atmdeficient mice. Cancer Res. 2001; 61:1849–54. [PubMed: 11280737]
45. Bakhoum SF, Danilova OV, Kaur P, et al. Chromosomal instability substantiates poor prognosis in patients with diffuse large B-cell lymphoma. Clin Cancer Res. 2011; 17:7704–11. [PubMed: 22184286]
46. van Gent DC, Hoeijmakers JHJ, Kanaar R. Chromosomal stability and the DNA double-stranded break connection. Nat Rev Genet. 2001; 2:196–206. [PubMed: 11256071]

47. Bunz F, Dutriaux A, Lengauer C, et al. Requirement for p53 and p21 to sustain G2 arrest after DNA damage. Science. 1998; 282:1497–501. [PubMed: 9822382]

48. Chen Z, Xiao Z, Chen J, Ng S-C, et al. Human Chk1 expression is dispensable for somatic cell death and critical for sustaining G2 DNA damage checkpoint. Mol Cancer Ther. 2003; 2:543–48. [PubMed: 12813133]

49. Igor BR, Eugenia VB, Bey-Dih C. If not apoptosis, then what? Treatment-induced senescence and mitotic catastrophe in tumor cells. Drug Resist Updat. 2001; 4:303–13. [PubMed: 11991684]

50. Castedo M, Perfettini J-L, Roumier T, et al. Cell death by mitotic catastrophe: a molecular definition. Oncogene. 2004; 23:2825–37. [PubMed: 15077146]

What's new?

Diffuse large B cell lymphoma (DLBCL) is a common malignancy that involves genomic instability and dysregulation of NF-κB signaling. Both canonical and noncanonical NF-κB signaling pathways play a role in DLBCL, acting either independently or concomitantly, though little is known about the noncanonical pathway. This study shows that noncanonical NF-κB signaling suppresses chromosome instability in DLBCL through the regulation of DNA damage and centrosome duplication. Those effects occurred via direct modulation of GADD45α, REDD1 and cyclin G2 expression. The data suggest that targeting noncanonical NF-κB activation could be an effective therapeutic strategy in DLBCL.

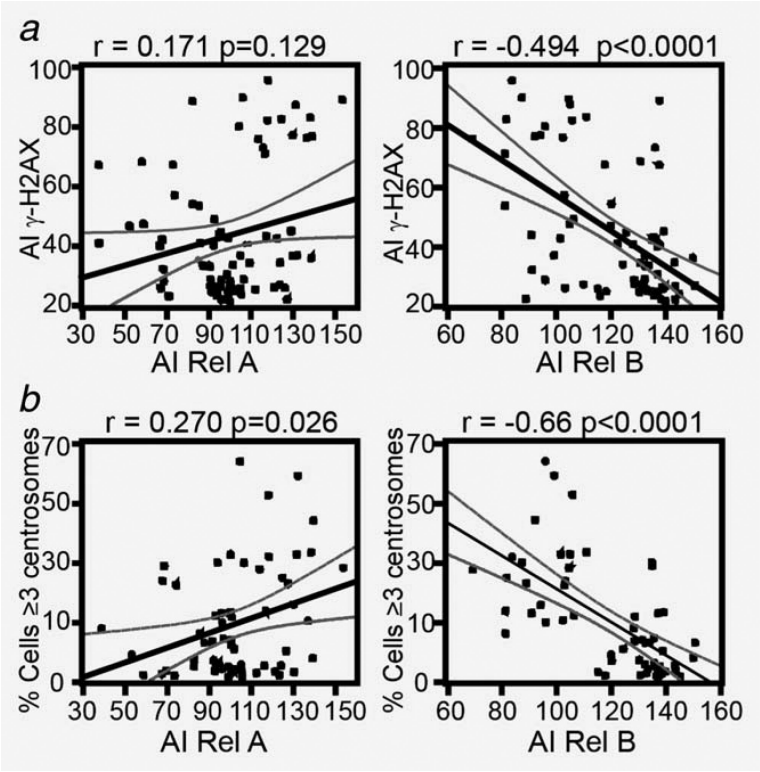

Figure 1.

Rel-B nuclear localization inversely correlates with DNA damage and centrosome amplification in DLBCL. Dot plots showing results of 92 lymph node samples from patients with DLBCL. (*a*) The correlation between the nuclear AI of Rel-A and Rel-B were compared to γ-H2AX AI using Spearman ranks correlation coefficient. (*b*) Correlation between the number of cells with centrosome amplification (≥3 centrosomes) and the AI signal of Rel-A and Rel-B. Centrosome counts were determined by manual count of at least 200 cells per image (four images per tissue).

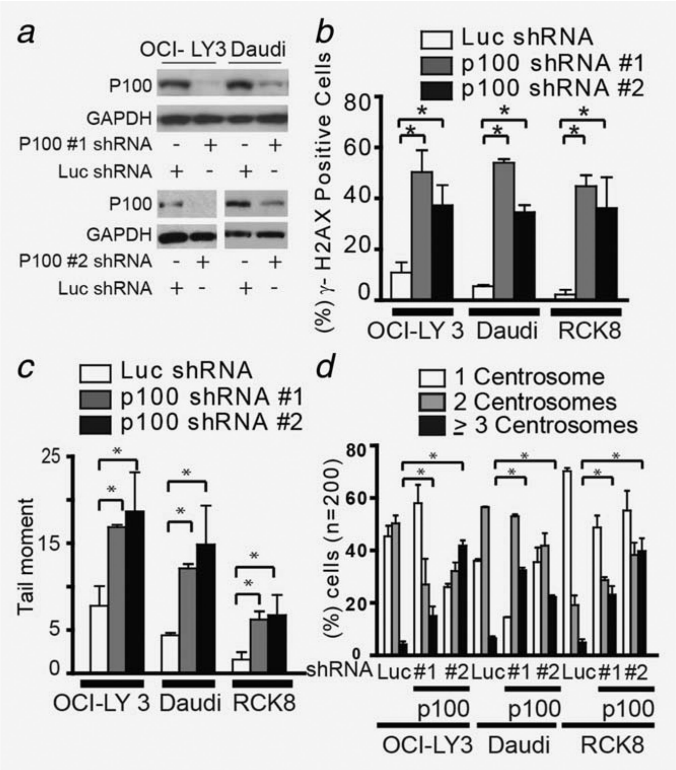

Figure 2.

Inhibition of the noncanonical NF-κB pathway results in DNA damage and centrosome amplification. (*a*) Protein levels of p100 in Daudi and OCI-LY3 cells expressing p100 (1 and 2)- and luciferase-shRNAs (Luc-shRNA). (*b*) Staining and quantification of γ-H2AX foci positive OCI-LY3 and Daudi cells expressing p100- and Luc-shRNA. Staining was performed after 2 weeks of growing cells in selection medium. Quantification was performed manually by counting a minimum of 200 cells in three different experiments. (*c*) Neutral comet assay of OCI-LY3 and Daudi expressing p100- and Luc-shRNA. The figure is representative of three independent experiments. OTM was used as an end point of DNA damage was measured in 100 cells. (*d*) Centrosome staining and quantification. Cells expressing p100- and Luc-shRNA were stained with anti-γ-tubulin and phospho-Aurora A. One way ANOVA was used for statistical analysis (*$p < 0.01$).

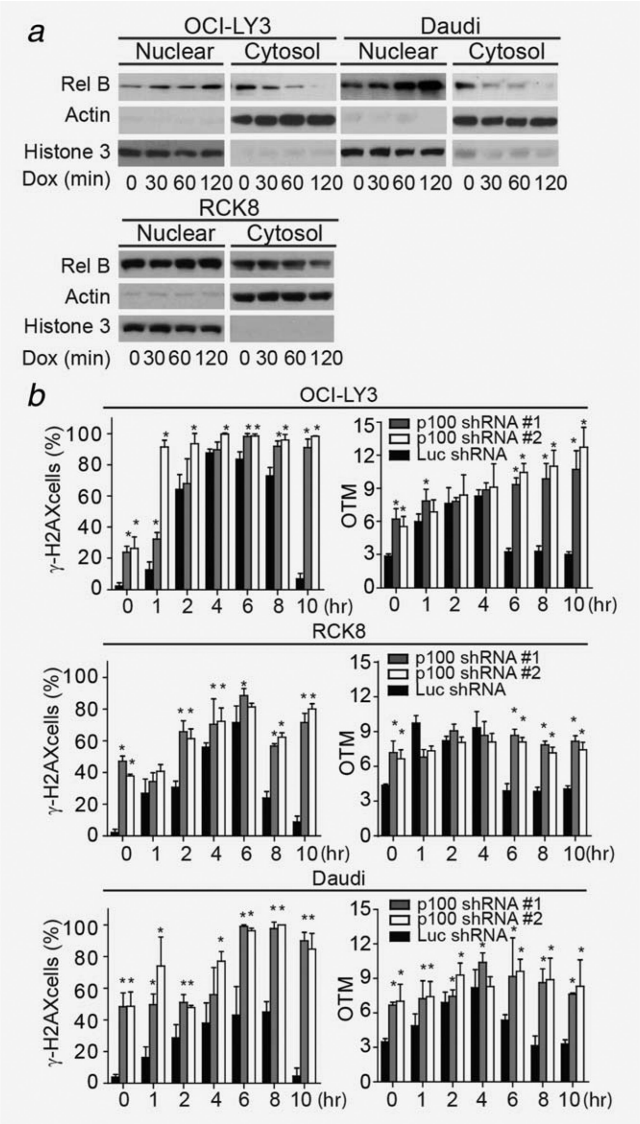

Figure 3.

Inhibition of the noncanonical pathway reduces DNA damage repair. (*a*) Effect of doxorubicin treatment on Rel-B nuclear localization. Nuclear and cytoplasmic fractions were extracted from OCI-LY3, RCK8 and Daudi cells at indicated time points after treatment with doxorubicin, followed by immunoblotting for Rel-B, Actin and histone 3. (*b*) Measurement of γ-H2AX (+) and OTM of OCI-LY3, RCK8 and Daudi cells expressing p100- or Luc-shRNA after doxorubicin treatment. Error bars represent the standard deviation obtained from three independent experiments. In (*b*) cells were harvested at different time points following 1 h treatment with doxorubicin (2 μg/mL). * $p < 0.01$.

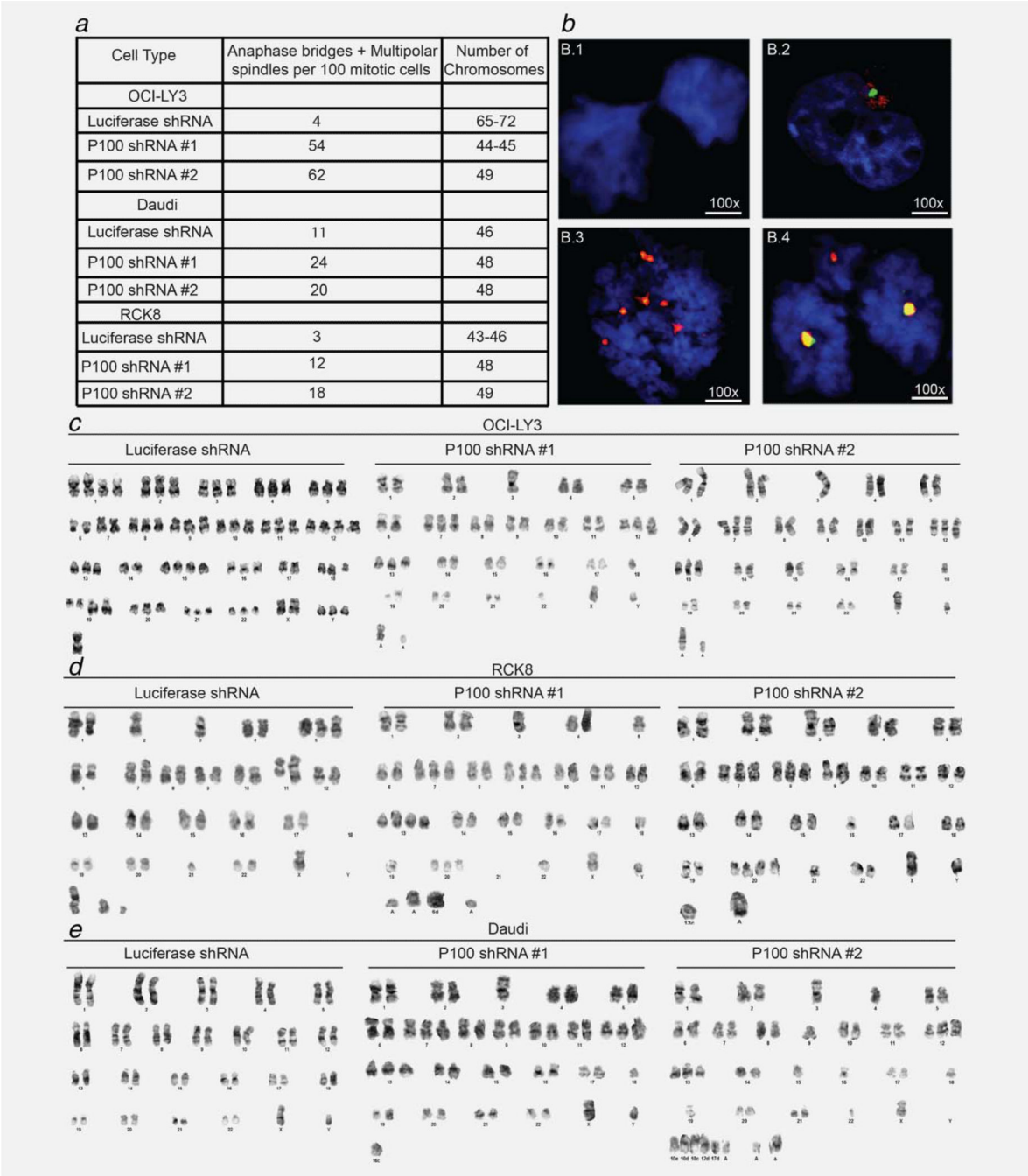

Cell Type	Anaphase bridges + Multipolar spindles per 100 mitotic cells	Number of Chromosomes
OCI-LY3		
Luciferase shRNA	4	65-72
P100 shRNA #1	54	44-45
P100 shRNA #2	62	49
Daudi		
Luciferase shRNA	11	46
P100 shRNA #1	24	48
P100 shRNA #2	20	48
RCK8		
Luciferase shRNA	3	43-46
P100 shRNA #1	12	48
P100 shRNA #2	18	49

Figure 4.

Silencing of p100 is associated with cleavage furrow defects and cytokinesis failure. (*a*) Table summarizing the number of abnormal anaphases and multipolar spindles observed in cells expressing p100- and Luc-shRNA. Centrosomes and mitosis were detected by costaining with anti-γ-tubulin and phospho-Aurora A. Anaphase bridges and multipolar spindles were quantified manually in 100 cells. (*b*) Index cases exemplifying: (*b.1*) anaphase bridge formation; (*b.2*) delay cleavage furrow and (*b.3* and *b.4*) multipolar anaphases (*p < 0.01). (*c*–*e*): Representative picture of metaphase spreads of control or silenced p100

expressing OCI-LY3, RCK8 and Daudi cells. Full karyotype analysis is shown in Supporting Information Table 1C.

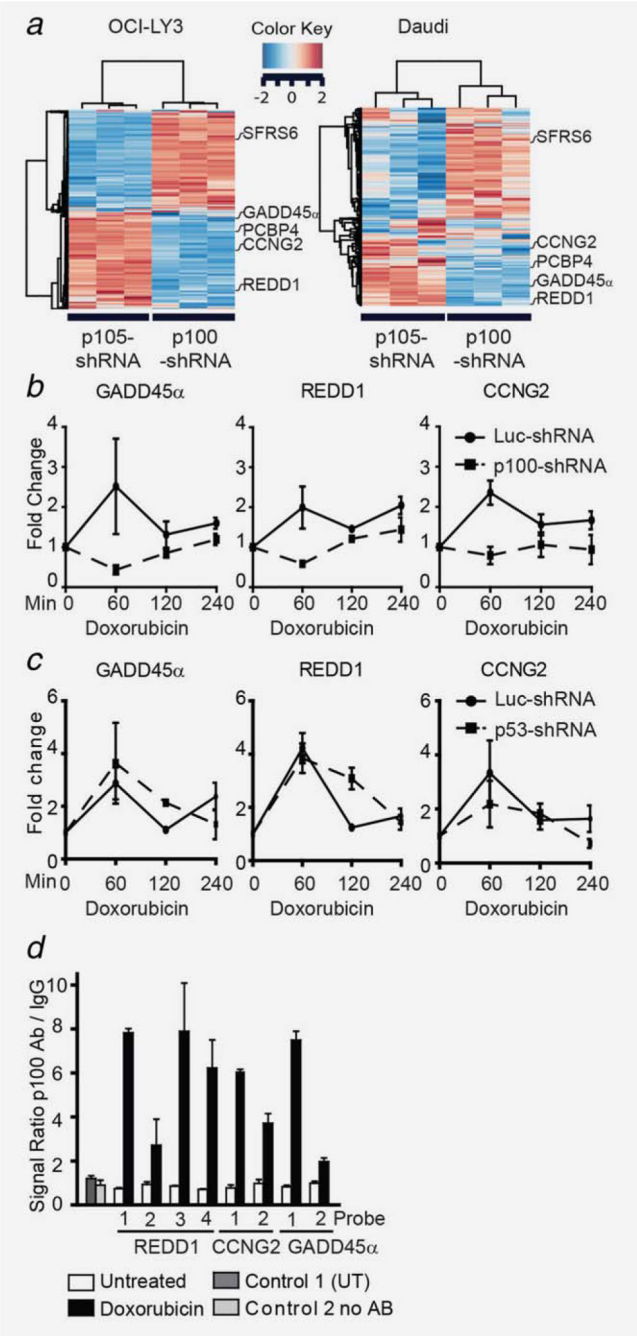

Figure 5.

The noncanonical NF-κB pathways directly regulate *GADD45α*, *REDD1* and *CCNG2*. Daudi and OCI-LY3 cells expressing p100-, p105- and luciferase-shRNA (Luc-shRNA) were grown in triplicate and RNA was extracted as described in the Materials and Methods section. (*a*) Heatmap illustrating the expression level of the top 300 genes distinguishing p100 from p105-regulated genes. (*b*) Changes in gene expression after doxorubicin treatment were measured by QPCR. Three independent experiments were used to extract RNA from OCI-LY3 cells expressing p100- (dashed line) or Luc-shRNA (solid line)

following a doxorubicin time course (2 μg/mL). (*c*) Changes in *GADD45α*, *REDD1* and *CCNG2* mRNA levels in luciferase (Luc)- or p53-shRNA expressing OCI-LY3 cells after 1 h of doxorubicin treatment. Each error bar is representative of the standard deviation of three independent experiments. (*d*) QCHIP assay of p100 targets. OCI-LY3 cells (50×10^6) were untreated or treated with doxorubicin for 60 min prior to fixation. Cells were prepared as described in the Materials and Methods section. Genomic QPCR was carried out in triplicate after DNA regions (numbered from 1–4) were immunoprecipitated (IP) with IgG or p100/p52 antibodies. Results are presented as a mean value with corresponding standard deviations. P100Ab = p100 antibody. All comparisons in this graph have $p < 0.001$. Control 1 = untranscribed region (UT), Control 2 = no antibody and Luc = Luciferase.

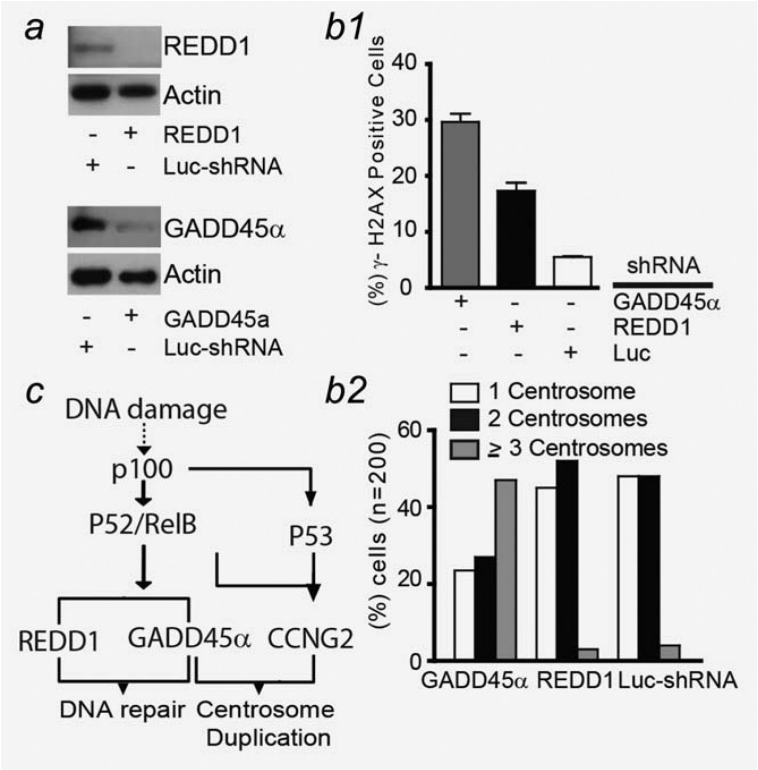

Figure 6.

(*a*) Protein levels of GADD45α and REDD1 in OCI-LY3 cells expressing GADD45α and REDD1-shRNA. Cells were fixed, processed and immunostained with anti-γ-H2AX (*b*.1) and γ-tubulin (*b*.2). Quantification was performed in 200 cells in three different experiments. (*c*) Schematic diagram of the NF-κB DNA damage response. Dashed line represents alternative unknown mechanisms of NF-κB activation induced by DNA damage.